Inverse Determination of Boundary Conditions and Sources in Steady Heat Conduction With Heat Generation

T. J. Martin

G. S. Dulikravich

Department of Aerospace Engineering,
Pennsylvania State University,
University Park, PA 16802

A Boundary Element Method (BEM) implementation for the solution of inverse or ill-posed two-dimensional Poisson problems of steady heat conduction with heat sources and sinks is proposed. The procedure is noniterative and cost effective, involving only a simple modification to any existing BEM algorithm. Thermal boundary conditions can be prescribed on only part of the boundary of the solid object while the heat sources can be partially or entirely unknown. Overspecified boundary conditions or internal temperature measurements are required in order to compensate for the unknown conditions. The weighted residual statement, inherent in the BEM formulation, replaces the more common iterative least-squares (L2) approach, which is typically used in this type of ill-posed problem. An ill-conditioned matrix results from the BEM formulation, which must be properly inverted to obtain the solution to the ill-posed steady heat conduction problem. A singular value decomposition (SVD) matrix solver was found to be more effective than Tikhonov regularization for inverting the matrix. Accurate results have been obtained for several steady two-dimensional heat conduction problems with arbitrary distributions of heat sources where the analytic solutions were available.

Introduction

The integrity of energy-producing or -consuming devices depends upon maintaining an acceptable operating temperature by the proper removal of generated heat. For example, Joule heating generated inside electronic components strongly depends on the frequency of the alternating electromagnetic field and the local material properties. Another example of such domain-distributed heat sources is the microwave heating of food and materials processing. In the case of buried nuclear or chemical toxic waste, the heat generated by ongoing reactions will vary throughout the burial site. In general, the internal heat generation may lead to local overheating, potentially serious equipment failures, and environmentally disastrous consequences. In order to understand the steady thermal field in these problems, a boundary value problem is often governed by the Poisson equation. A well-posed problem requires either temperature, heat flux, or convective heat transfer coefficients specified over the entire boundary of the solid region. Well-posed Poisson problems also require the specification of heat source intensities throughout the domain.

However, surface measurements and continuous monitoring of the heat sources throughout the solid are often impractical. This is because of the intrusive nature of a large number of sensors. In addition, using even a small number of sensors may be impossible to achieve in practice because of highly volatile environments (combustion chambers) or because of the prohibitively small space available for their placement (computer chips). Thus, in many cases we are forced to solve an ill-posed boundary value problem where no data are available on parts of the boundary or when the heat sources are partially or entirely unknown. It would be highly desirable to develop a nonintrusive monitoring technique capable of utilizing overdetermined thermal measurements where they are accessible to the designer. The overspecified boundary conditions would then be used to predict temperatures, heat fluxes, and convective heat transfer coefficients on the inaccessible boundaries. This objective is termed the steady inverse heat conduction problem (SIHCP).

We have developed a noniterative algorithm that can reliably and efficiently solve inverse (ill-posed) boundary condition problems governed by the Laplace equation in two-dimensional multiply connected domains including temperature-dependent material properties (Martin and Dulikravich, 1993, 1994; Dulikravich and Martin, 1994). An extended version of this method was also successfully used in solving ill-posed problems in two-dimensional elasticity (Martin et al., 1994). In the latter publication, no boundary conditions for traction and deformation were known on parts of the boundary while both traction and deformation vectors were specified on the remainder of the boundary of the multiply connected domain.

In this paper, the problem formulation is conceptually different from the more common unsteady inverse heat conduction problem (UIHCP) (Beck et al., 1984). The major concern when attempting to solve the UIHCP computationally has been with the automatic filtering of noisy data in the discrete thermocouple measurements. All measurement data errors, as well as numerical round-off errors, are amplified by the typical UIHCP algorithms. These numerical methods are usually formulated in the least-squares sense where the overall error between the computed and measured temperatures is minimized (Kagawa et al., 1995). Among others, the method of regulizers, discrete mollification (Murio, 1993) against a suitable averaging kernel and other filtering techniques have also been implemented in order to smooth the extrapolated boundary values. To date, many of the UIHCP solutions were performed for specific geometries and cannot be readily extended to complex geometries.

Contributed by the Heat Transfer Division for publication in the JOURNAL OF HEAT TRANSFER. Manuscript received by the Heat Transfer Division April 1995; revision received March 1996. Keywords: Computer Codes, Conduction, Numerical Methods. Associate Technical Editor: S. Ramadhyani.

In fact, most attention has been focused on the one-dimensional UIHCP. Another basic concern is that relatively few UIHCP techniques used in engineering provide a quantitative method for determining what effect their smoothing operations have on the accuracy of the estimates.

The theory behind our SIHCP method is based on the Green's function solution method, commonly referred to as the Boundary Element Method (BEM). It is an integral technique that generates a set of linear algebraic equations with unknowns confined only to the boundaries. For well-posed problems, the resulting solution matrix can be solved by Gaussian elimination or any other standard matrix inverter. When an ill-posed problem is encountered, the matrix becomes ill-conditioned. We have shown that the proper solution to this matrix provides accurate results to various SIHCPs. This method has been shown to suppress the amplification in measurement errors (Martin and Dulikravich, 1994) in the input data while both minimizing the variance in the output and preventing output bias. The approach is somewhat similar, at least in theory, to those delivered by Backus and Gilbert (1970) and Lanczos (1961). These authors have discussed techniques that allow one to selectively discard eigenvalues and eigenvectors of a particular system of equations that tend to magnify errors.

Numerical Formulation

This paper elaborates on a simple, robust, and fast numerical solution to the ill-posed two-dimensional Poisson equation using the BEM. The algorithm is applicable to complex, multiply connected, two and three-dimensional geometries. The BEM (Brebbia, 1978) is based upon a Green's function solution procedure. It has certain distinct advantages over other more common numerical methods. First, the analytic solution to the partial differential equation, in the form of the Green's function, is part of the BEM solution. Therefore, high accuracy is expected with the BEM because introducing the Green's functions does not introduce any error into the solution. In addition, the BEM does not, like the Finite Element Method (FEM), neglect the interelement continuity terms. Third, the degrees of freedom of the system are reduced such that unknowns are strictly confined to the boundaries of the domain. Most importantly, the noniterative nature of the BEM eliminates stability and convergence problems.

The governing partial differential equation for steady-state heat conduction in a two-dimensional solid with a constant coefficient of thermal conductivity, and arbitrarily distributed heat sources or sinks per unit area is

$$k\nabla^2 T(\mathbf{x}) + g(\mathbf{x}) = 0 \tag{1}$$

This equation can be nondimensionalized by introducing

$$u = \frac{T - T_{\min}}{(T_{\max} - T_{\min})} \quad b = \frac{gl^2}{k(T_{\max} - T_{\min})} \tag{2}$$

where l is a characteristic length. The nondimensional form of Eq. (1) then becomes

$$\nabla^2 u(\mathbf{x}) + b(\mathbf{x}) = 0 \tag{3}$$

This elliptic partial differential equation can be subject to the Dirichlet boundary conditions, $u = \bar{u}_1$, on the boundaries Γ_1, the Neumann boundary conditions, $\partial u/\partial n = \bar{q}_2$, on the boundaries Γ_2, and, when a boundary is exposed to a moving fluid, the Robin (convective heat transfer) boundary conditions, $-k(\partial u/\partial n) = h(\bar{u} - u_{\text{amb}})_3$, on the boundaries Γ_3. When an ill-posed boundary condition problem is encountered, the boundaries Γ_4 have both $u = \bar{u}_4$ and $q = \bar{q}_4$ specified, while nothing is known on boundaries Γ_5, that is, $\bar{u}_5$ = unknown and $\bar{q}_5$ = unknown.

Boundary Element Method. When a partial differential equation is formulated numerically, an approximate solution, which is, in general, not the exact solution, must be used. Therefore, error, often called the residual, is introduced into the problem. The weighted residual statement minimizes this error by

Nomenclature

$[\mathbf{A}]$ = coefficient matrix multiplying a vector of unknowns
A_{nm} = Fourier sine coefficients
b = nondimensional internal heat source function
$\{\mathbf{B}\}$ = vector of nodal nondimensional heat sources
B_{nm} = Fourier cosine coefficient
$[\mathbf{C}]$ = SVD matrix whose columns are an orthonormal basis that spans the range of $[\mathbf{A}]$
$[\mathbf{D}]$ = SVD matrix whose columns are an orthonormal basis for the nullspace of $[\mathbf{A}]$
E = error
$\{\mathbf{F}\}$ = vector of known sources and boundary conditions
g = internal heat source per unit domain
$[\mathbf{G}]$ = BEM coefficient matrix multiplying nodal fluxes
h = convective heat transfer coefficient
$[\mathbf{H}]$ = BEM coefficient matrix multiplying nodal potentials
$[\mathbf{I}]$ = identity matrix
J_n = Bessel function of integer order n
k = coefficient of thermal conductivity
n = local outward unit normal direction
$\hat{n}$ = local outward unit normal vector
N = number of nodes
$[\mathbf{P}]$ = BEM coefficient matrix multiplying nodal sources
q = nondimensional flux
$\{\mathbf{Q}\}$ = vector of nodal nondimensional fluxes
R = random number with uniform distribution between 0.0 and 1.0
T = temperature
u = nondimensional temperature or potential
$\{\mathbf{U}\}$ = vector of nodal potentials
w = weighting function
$\mathbf{x}$ = real space coordinate (x_1, x_2)
$\mathbf{y}$ = coordinate of integration (y_1, y_2)
Y_n = Bessel function of integer order n
Γ = boundary contour
δ = Dirac delta function
θ = circumferential angle
λ = Tikhonov regularization parameter
μ_{nm} = roots of the characteristic equation
ρ = nondimensional radius
σ = standard deviation
σ^2 = variance
τ = singularity threshold
Ω = domain

Subscripts

a = inner circular boundary
amb = ambient fluid quantities
b = outer circular boundary
int = internal temperature measurement
j = column index of coefficient matrix A
max = maximum value of temperature
min = minimum value of temperature
opt = optimum value
T = temperature
vc = domain cells
1 = Dirichlet boundary condition
2 = Neumann boundary condition
3 = Robin boundary condition
4 = overspecified boundary conditions
5 = nonspecified boundary condition

Superscripts

$*$ = fundamental Green's function
T = transpose of a matrix
-1 = inverse of a matrix

setting the weighted sum of the residuals over the entire domain and in the boundary conditions to zero. For the Poisson equation, the weighted residual statement appears as

$$\int_\Omega (\nabla^2 u(\mathbf{y}) + b(\mathbf{y}))w(\mathbf{x}, \mathbf{y})d\Omega(\mathbf{y}) + \int_{\Gamma_1} (u(\mathbf{y}) - \bar{u}(\mathbf{y})) \frac{\partial w(\mathbf{x}, \mathbf{y})}{\partial n} d\Gamma(\mathbf{y}) - \int_{\Gamma_2} (q(\mathbf{y}) - \bar{q}(\mathbf{y}))w(\mathbf{x}, \mathbf{y})d\Gamma(\mathbf{y}) = 0 \quad (4)$$

This statement is the starting point of most numerical formulations. The difference among them lies in how the weighting function is formulated and what approximating function is used.

In the BEM, the fundamental Green's function solution, which will be represented by u^*, replaces the weighting function, w. It satisfies the following Green's function solution equation with a unit impulsive heat source and homogeneous boundary conditions:

$$\nabla^2 u^* + \delta(\mathbf{x} - \mathbf{y}) = 0 \quad (5)$$

The Dirac delta function, $\delta(\mathbf{x} - \mathbf{y})$, has the following property:

$$\int_\Omega f(\mathbf{y})\delta(\mathbf{x} - \mathbf{y})d\Omega = \begin{cases} 0 & \text{when } \mathbf{x} \text{ is outside } \Omega \\ f(\mathbf{x}) & \text{when } \mathbf{x} \text{ is inside } \Omega \end{cases} \quad (6)$$

The nondimensional steady heat conduction equation Eq. (3), enters into the first integral of Eq. (4). The nondimensional heat flux is defined as $q = \partial u/\partial n$. After integrating the weighted residual statement (4) by parts twice, retaining the Cauchy principal value of the boundary integrals, and using the properties of the Dirac delta function (Eqs. (5) and (6)), the following Boundary Integral Equation (BIE) is obtained (Brebbia and Dominguez, 1989):

$$c(\mathbf{x})u(\mathbf{x}) + \int_\Gamma q^*(\mathbf{x}, \mathbf{y})u(\mathbf{y})d\Gamma = \int_\Gamma u^*(\mathbf{x}, \mathbf{y})q(\mathbf{y})d\Gamma + \int_\Omega u^*(\mathbf{x}, \mathbf{y})b(\mathbf{y})d\Omega \quad (7)$$

The fundamental solution for the two-dimensional Poisson equation is

$$u^* = \frac{1}{2\pi} \ln\left(\frac{1}{|\mathbf{x} - \mathbf{y}|}\right) \quad (8)$$

The boundary integral is singular when the observation point, $\mathbf{x}$, is on the boundary. Therefore, these singular integrals must be evaluated in the sense of the Cauchy principal value. The integration over the boundary, Γ, is divided into an infinitesimal semicircular contour, Γ_ϵ, about the singular point plus the remaining contour, $\Gamma - \Gamma_\epsilon$. After taking the limit $\epsilon \to 0$, a free term, $c(\mathbf{x})u(\mathbf{x})$, results. For two-dimensional problems, $c(\mathbf{x}) = 0.0$ when $\mathbf{x}$ is outside the domain, $c(\mathbf{x}) = 1.0$ when $\mathbf{x}$ is inside the domain, and $c(\mathbf{x}) = \theta/2\pi$ when $\mathbf{x}$ is on the boundary, where θ is the internal angle at the corner between two neighboring boundary elements.

If the temperature gradient is known at some location in the domain, the following BIE can be derived:

$$\nabla u(\mathbf{x}) + \int_\Gamma \nabla q^*(\mathbf{x}, \mathbf{y})u(\mathbf{y})d\Gamma = \int_\Gamma \nabla u^*(\mathbf{x}, \mathbf{y})q(\mathbf{y})d\Gamma + \int_\Omega \nabla u^*(\mathbf{x}, \mathbf{y})b(\mathbf{y})d\Omega \quad (9)$$

The boundary was discretized into N linear, isoparametric, boundary elements connected at N boundary nodes. In addition, N_{int} internal points existed where temperature data were specified. Since the boundary elements were isoparametric, the functions u and q varied linearly between their values at the end-points (nodes) of each boundary element. Each boundary element, Γ_j, was integrated numerically using a standard Gaussian quadrature integration formula. Boundary elements containing a singularity at one end-point were integrated analytically. A set of $N + N_{int}$ boundary integral equations resulted, one for each boundary node plus one for every internal temperature measurement. In order to evaluate the field source integral, the domain, Ω, was discretized into N_{vc} quadrilateral, isoparametric bilinear cells, Ω_j, sharing both domain and boundary nodes at the vertices of these quadrilaterals.

The coefficients matrices $[\mathbf{H}]$, $[\mathbf{G}]$, and $[\mathbf{P}]$ were computed by integrating the fundamental solution over the linear boundary elements and over the bilinear domain elements. The resulting discretized form of the BIE can be represented in matrix form as follows (Dulikravich and Martin, 1995):

$$[\mathbf{H}]\{\mathbf{U}\} = [\mathbf{G}]\{\mathbf{Q}\} + [\mathbf{P}]\{\mathbf{B}\} \quad (10)$$

For a well-posed boundary value problem, every point on the boundary is given one Dirichlet, Neumann, or Robin-type boundary condition, no internal temperature measurements exist, and the heat source vector $\{\mathbf{B}\}$ is entirely known. These boundary conditions are then multiplied by their respective coefficient matrix, collected on the right-hand side and added to $[\mathbf{P}]\{\mathbf{B}\}$ to form a vector of knowns, $\{\mathbf{F}\}$. The left-hand side will remain in the standard form $[\mathbf{A}]\{\mathbf{X}\}$, with the matrix $[\mathbf{A}]$, having N unknowns and N equations. This well-posed system of linear algebraic equations can be solved for the unknowns on the boundary by any standard matrix solver such as Gaussian elimination of LU factorization.

If the boundary conditions in the example above are partially unknown or not properly applied, if internal temperature measurements are included in the analysis, or if part or all of the heat source function is unknown, the problem becomes ill-posed. A solution may still be obtained by multiplying the known quantities in the vectors $\{\mathbf{U}\}$, $\{\mathbf{Q}\}$, and $\{\mathbf{B}\}$ by their respective coefficient matrix columns and collecting them into the vector of knowns. The unknowns form a single vector, $\{\mathbf{X}\}$, multiplied by a highly ill-conditioned coefficient matrix, $[\mathbf{A}]$, which is, in general, not square.

Singular Value Decomposition. Singular Value Decomposition (SVD) methods (Press et al., 1992; Throne and Olson, 1994; Sykulski, 1995) are widely used for dealing with sets of algebraic equations that are either singular or very close to singular. The goal of the SVD is to choose a solution vector $\{\mathbf{X}\}$ that minimizes the error function

$$E = \|\{\mathbf{F}\} - [\mathbf{A}]\{\mathbf{X}\}\| \quad (11)$$

which is the distance from the point $\{\mathbf{F}\}$ to the point $[\mathbf{A}]\{\mathbf{X}\}$ in the column space. Any $M \times N$ matrix $[\mathbf{A}]$ can be written as the product of an $M \times N$ column-orthogonal matrix, $[\mathbf{C}]$, an $N \times N$ diagonal matrix $[\mathbf{S}]$ with positive singular values, and the transpose of an $N \times N$ orthogonal matrix $[\mathbf{D}]$.

$$[\mathbf{A}] = [\mathbf{C}] \begin{bmatrix} s_1 & 0 & 0 \\ 0 & \vdots & 0 \\ 0 & 0 & s_N \end{bmatrix} [\mathbf{D}] \quad (12)$$

The singular values, $s_1, s_2, \ldots, s_N$, are the eigenvalues of matrix $[\mathbf{A}]^T[\mathbf{A}]$. For a well-conditioned matrix, these values will be roughly of the same order of magnitude. As the matrix becomes more ill-conditioned, that is, more singular, these values become more dispersed. Formally, the condition number of a matrix is defined as the base 10 logarithm of the ratio between the largest of the s_j's to the smallest of the s_j's.

The SVD explicitly constructs orthonormal bases for the nullspace and range of a matrix [A]. If the matrix [A] is singular, then there is some subspace of {X}, called the nullspace, that is mapped to zero, that is, [A]{X} = {0}. The LU factorization and Gaussian elimination techniques may give a formal solution to an ill-conditioned set of equations, but the solution vector {X} will have highly oscillating components. When this solution vector, {X}, is multiplied by the matrix [A], a very poor approximation to the vector {F} will be the result.

Eliminating very small singular values has the effect of removing those algebraic terms that, because they are dominated by noise and round-off error, corrupt the solution. In order to determine which singular values are to be truncated, we must choose a parameter, τ, as a singularity threshold. Any singular value, whose ratio with the largest singular value is less than this singularity threshold, is zeroed out. This can be understood as follows: If $s_j/s_{\max} < \tau$, then $1/s_j = 0$.

Since [C] and [D] are each orthogonal in the sense that their columns are orthonormal, the solution vector can be easily found as

$$\{\mathbf{X}\} = [\mathbf{D}][\mathrm{diag}(1/s_j)]([\mathbf{C}]^T\{\mathbf{F}\}) \quad (13)$$

Tikhonov Regularization. Another type of single-parameter minimization where the solution vector {X} minimizes the weighted sum of the norm of the error vector plus a penalty term was defined by Tikhonov (1977) as

$$E = \|\{\mathbf{F}\} - [\mathbf{A}]\{\mathbf{X}\}\| + \lambda\|\{\mathbf{X}\}\| \quad (14)$$

We find a minimum error norm by differentiating this equation with respect to each component of the unknown vector, {X}, and setting the result equal to zero. After substituting the singular value decomposition and solving for the unknown vector {X}, the resulting formulation is as follows:

$$\{\mathbf{X}\} = [\mathbf{D}]([\mathbf{S}]^T[\mathbf{S}] + \lambda[\mathbf{I}])^{-1}[\mathbf{S}]^T\{\mathbf{C}\}\{\mathbf{F}\} \quad (15)$$

Tikhonov regularization is a generalization of least-squares truncation, but instead of simply eliminating terms associated with small singular values, they are weighted by a factor $(1 + \lambda/s^2)$. The Tikhonov regularization parameter, λ, plays an important role. A low value drives the residual term [A]{X} − {F} smaller, approaching the least-squares solution. Because of the destabilizing effect of the small singular values, the solution for an ill-conditioned matrix oscillates erratically. Larger Tikhonov regularization parameters act as a filter to gradually reduce the effect of the singular values because $s_j/s_{\max}$ are less than the regularization parameter, λ. Thus, the optimal choice of the regularization parameter provides a balance between the accuracy and the smoothness of the solution. Tikhonov suggested that this parameter can be found based upon knowledge of the input measurement errors (Beck et al., 1985). The optimum value of λ should be chosen so that the variance in the output vector is at its minimum.

Analytic Test Cases. The two-dimensional BEM algorithm was verified against the analytic solution for the heat conduction equation within an annular region. If the boundary conditions and the heat generation in the annular domain are axisymmetric, $b = b(\rho)$, then the temperature distribution is

$$u(\rho) = -\int\left[\frac{1}{\rho}\int b(\rho)\rho d\rho\right]d\rho + c_1 \ln \rho + c_2 \quad (16)$$

In case of a constant heat source function (b = constant) the analytic solution of Eq. (16) is

$$u = -b\frac{\rho^2}{4} + c_1 \ln \rho + c_2 \quad (17)$$

where the constants of integration c_1 and c_2 can be found after applying the boundary conditions.

The temperature distribution within an annular domain with an arbitrary heat source distribution, $b = b(\rho, \theta)$ was also needed as a test case. For this problem, the inner circular boundary of the annular domain had a Dirichlet boundary condition, $u(\rho_a) = 0$, while the outer circular boundary was adiabatic. We can obtain an eigenfunction set written in the form of the Helmholtz equation satisfying the homogeneous boundary conditions. After separation of variables and applying the single-valuedness condition, the analytic result for the temperature field in the annular domain is

$$u(\rho, \theta) = \sum_{n=0}^{\infty}\sum_{m=1}^{\infty}\left[J_n(\mu_{nm}\rho) - \frac{J_n(\mu_{nm}\rho_b)}{Y_n(\mu_{nm}\rho_b)}Y_n(\mu_{nm}\rho)\right] \times [A_{nm}\sin n\theta + B_{nm}\cos n\theta] \quad (18)$$

The Fourier coefficients, A_{nm} and B_{nm}, may be found knowing that the eigenfunctions form an orthogonal set. Here, J_n and Y_n are the Bessel functions of integer order n, and μ_{nm} are the roots of the characteristic equation (Dulikravich and Martin, 1995):

$$J_n\left(\mu_{nm}\frac{\rho_{\text{outer}}}{\rho_{\text{inner}}}\right)Y_n'(\mu_{nm}) - J_n'(\mu_{nm})Y_n\left(\mu_{nm}\frac{\rho_{\text{outer}}}{\rho_{\text{inner}}}\right) = 0 \quad (19)$$

Results

Our inverse BEM algorithm governing the Poisson equation was tested against the analytic solution for an annular, homogeneous, isotropic, planar region between two concentric circles with nondimensionalized radii $\rho_a = 0.5$ and $\rho_b = 1.2$ subject to axisymmetric nondimensional thermal boundary conditions (u_a and u_b) and constant nondimensional heat generation function, b.

Effects of Discretization. In the first test case no heat sources, ($b = 0$), were applied. Equation (17) gives an analytic solution for the well-posed problem, $u_a = 0.5$ and $u_b = 1$, that results in the analytic values of $q_a = -1.134$ and $q_b = 0.4976$. The outer boundary was then overspecified with both constant nondimensional temperature and flux boundary conditions ($u_b = 1$, $q_b = 0.4976$) taken from the analytic solution of the well-posed problem, while nothing was specified on the inner circular boundary. Each outer and inner circular boundary was discretized with a variable, $N_a = N_b = M/2$, isoparametric linear boundary elements connected between the same number of nodes. Various levels of discretization were employed such that $M/2$ = 12, 24, 36, 48, 72, 84 and 144. Each BEM solution matrix was square, ($M \times M$), all had very similar ranges of singular values and the condition number of each matrix was between 7 and 8. The variances in the output temperatures (computed on the inner boundary),

$$\sigma_T^2 = \sum_{j=1}^{M/2}(u_j - u_{\text{mean}})^2 \quad (20)$$

where u_{mean} is the mean value, were examined for a range of singularity thresholds, τ, and a range of Tikhonov regularization parameters, λ, varying between 1 and 10^{-16}. The idea is to find the optimum value, τ_{opt} or λ_{opt}, that simultaneously minimizes the output variance and the bias.

The computed nondimensional temperature and flux distributions on the inner circular boundary were very accurate, approaching the analytic solution with the increasing level of discretization. Figure 1 illustrates the effect of the user-specified singularity threshold, τ, on the computed nondimensional temperature variances on the inner circular boundary for a range of discretization levels. The bias (difference between computed u_{mean} and the analytic solution) in the results approached zero as the level of discretization increased while the output variance reached a minimum at about $M/2 = 36$ linear boundary ele-

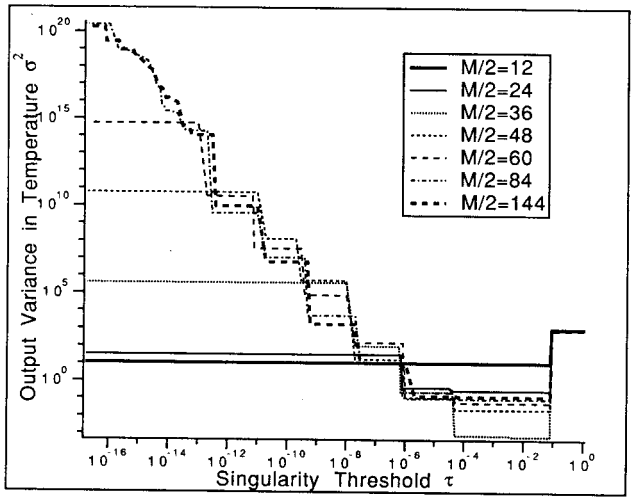

Fig. 1 Variances in the output (computed inner boundary) nondimensional temperatures as a function of the SVD singularity thresholds, τ. A range of M/2 boundary elements were used to discretize each circular boundary of the annular region.

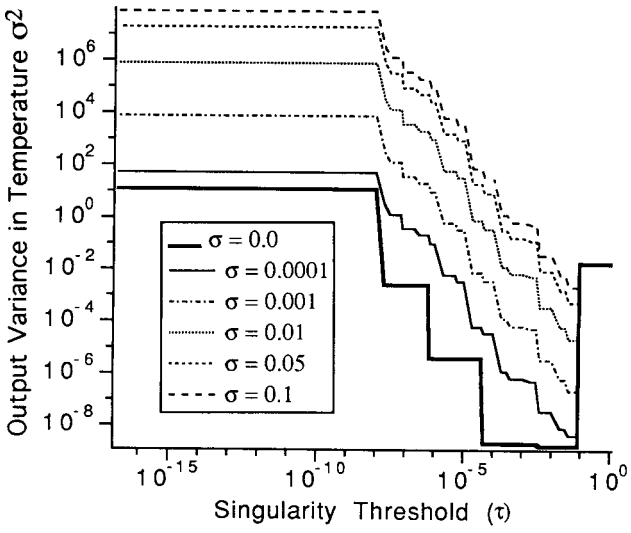

Fig. 2 Variances in the output (computed inner boundary) nondimensional temperatures and heat fluxes as a function of the SVD singularity threshold parameter, τ, for various levels of input standard deviation, σ

ments per circular boundary. This bias was, therefore, attributed to the fact that linear elements were used to model the circular geometry. The level of discretization was found to have no effect on τ_{opt}. The effective range of τ that produced the minimum variance and bias for all levels of discretization was $0.004 \leq \tau \leq 0.08$.

On the other hand, the level of discretization had some influence on Tikhonov's regularization scheme. After the BEM matrices were integrated and the singular value decomposition computed, an iterative quadratic optimization algorithm was employed in order to determine λ_{opt}. The value of λ was allowed to vary while the cost function

$$f(\lambda) = w_{var}\sigma_T^2 + w_{bias}(u_{mean} - u_{analytic})^2 \qquad (21)$$

was minimized. Here w_{var} and w_{bias} are user-specified weighting coefficients for the variance and the bias. With $w_{var} = w_{bias} = 1$, the optimum Tikhonov regularization parameter was usually found in 5 to 10 computationally inexpensive iterations.

Results With Input Data Noise. The major concern of researchers working on inverse problems is with the sensitivity of their algorithms to errors in the specified boundary conditions. In order to verify that our SIHCP technique did not amplify the input data errors, random Gaussian noise was introduced into the temperature function supplied to the outer circular boundary. The same annular geometry was used for this purpose and the heat generation was included as a constant, $b = 1$. For the temperature boundary condition on the outer boundary a uniform random real number, R, between 0 and 1, was generated using the RANF subroutine on the Cray C-90 computer. Using this value as the normalized probability density function, a noisy temperature boundary condition on the outer circular boundary was determined from the following equation:

$$u(\theta) = u_{bc} \pm \sqrt{-2\sigma^2 \ln [R(\theta)]} \qquad (22)$$

The sign was determined by generating another random number with a 50/50 chance of being +/−. Here, $u_{bc} = u_b = 0$, is the mean value of the temperature boundary condition on the outer circular boundary and σ^2 is the variance. With $u_b = u_a = 0$ and $b = 1$ the analytic solution of the well-posed problem was obtained from Eq. (17) with $c_1 = 0.3398$ and $c_2 = 0.298$ yielding a maximum nondimensional temperature, $u_{max} = 0.06248$, reached at the nondimensionalized radial distance $\rho = 0.8244$. The analytic solution also gives $q_a = 0.4296$ and $q_b = -0.3168$. For the inverse problem, no boundary conditions were specified on the inner circular boundary while specifying $u_b = 0$ and $q_b = -0.3168$ on the outer circular boundary. Each circular boundary was discretized with $M/2 = 36$ boundary elements. Ten rows of quadrilateral cells discretized the circular annular domain.

Our SIHCP BEM program was then tested with a variety of input nondimensional temperature standard deviations, σ, on the outer boundary. The ill-conditioned solution matrices were solved using the SVD algorithm and Tikhonov's regularization scheme. In order to determine τ_{opt} and and λ_{opt} for each case. Figs. 2 and 3 were generated to illustrate the behavior of these parameters. Each figure shows the output variance in temperature versus the range of possible τ's and λ's between 10^{-16} and 1. Notice that τ_{opt} is not a function of the input σ, but λ_{opt} is.

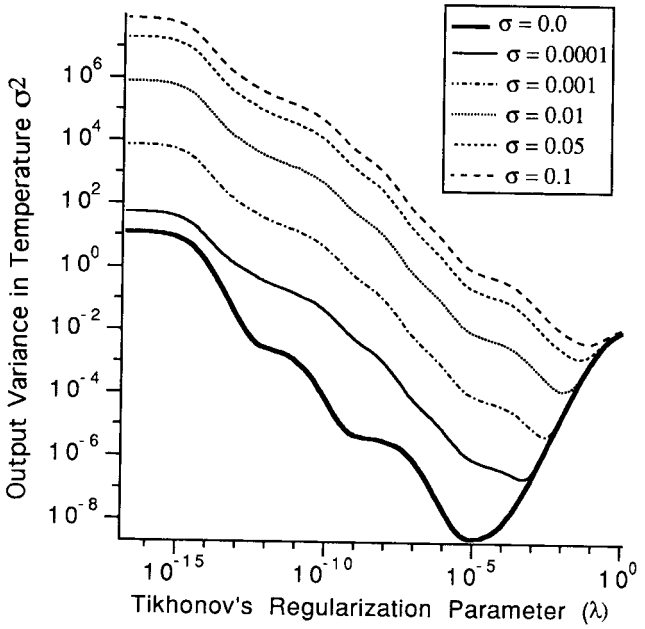

Fig. 3 Variances in the output (computed inner boundary) nondimensional temperatures and heat fluxes as a function of the Tikhonov's regularization parameter, λ. The curves are shown for various levels of input standard deviation, σ.

The optimum SVD threshold, τ_{opt}, which occurs when the variances in the output (inner circular boundary) nondimensional temperatures and heat fluxes are minimized, remained relatively constant and independent of all levels of input standard deviations. The input standard deviations, between $0 \leq \sigma \leq 0.1$, corresponding to errors from 0 up to 100 percent or more, yielded a minimum output variance when the singularity threshold, τ_{opt}, was $0.04 \leq \tau \leq 0.08$. The value of λ_{opt} was found by the iterative optimization process described earlier.

With the optimum SVD threshold and Tikhonov's regularization parameters known, Figs. 4, 5, and 6 were generated to depict the influence of the input percent errors supplied to the outer boundary conditions in temperature (solid lines) and the percent errors computed by the program as the inner boundary

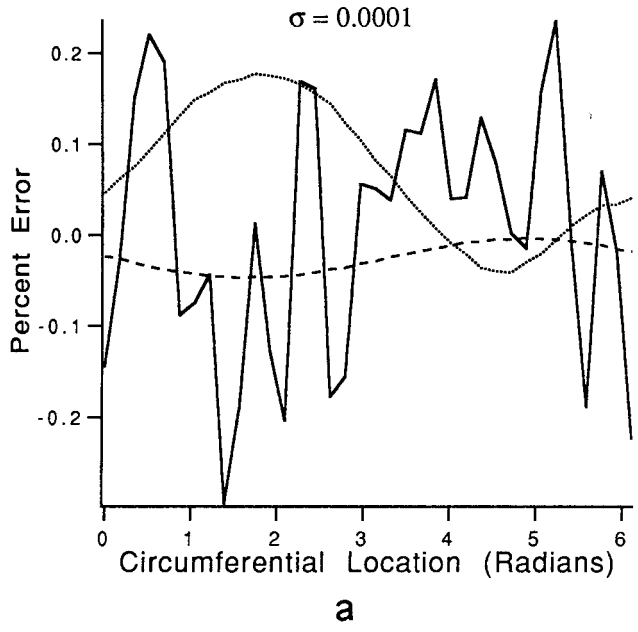

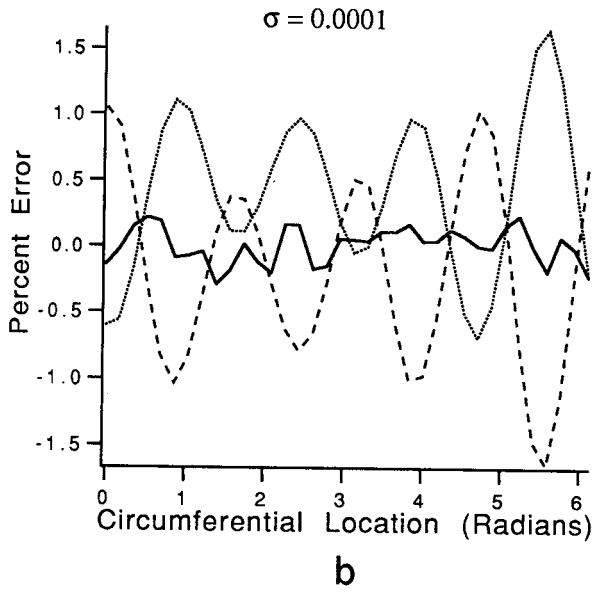

Fig. 4 Circumferential distribution of specified (input) percentage errors of nondimensional temperature on the outer circular boundary (full line) and computed (output) percentage errors in nondimensional temperature (dotted line) and heat flux (dashed line) on the inner circular boundary: (*a*) using the SVD algorithm, and (*b*) using Tikhonov's regularization. Input standard deviation was $\sigma = 0.0001$.

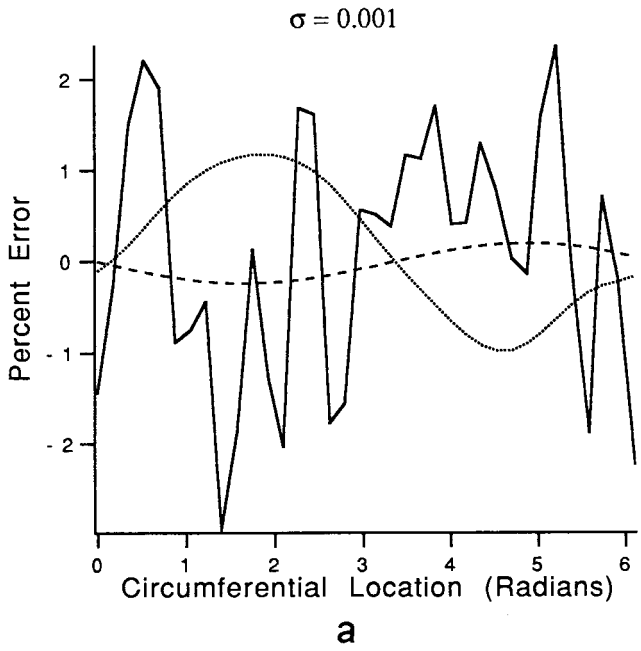

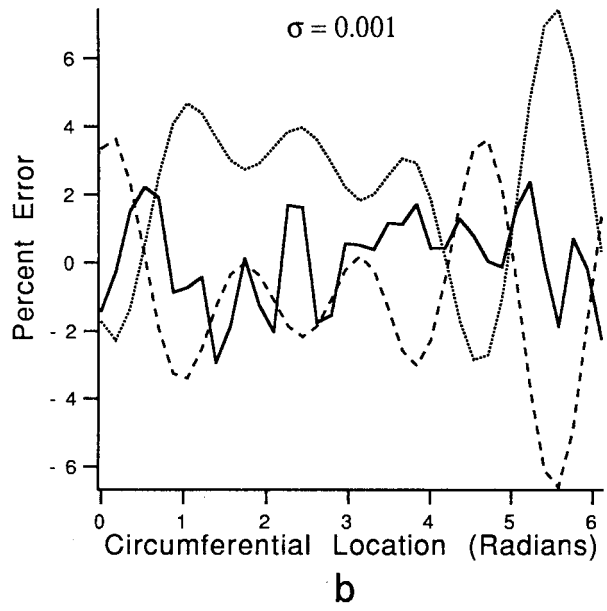

Fig. 5 Circumferential distribution of specified (input) percentage errors of nondimensional temperature on the outer circular boundary (full line) and computed (output) percentage errors in nondimensional temperature (dotted line) and heat flux (dashed line) on the inner circular boundary: (*a*) using the SVD algorithm, and (*b*) using Tikhonov's regularization. Input standard deviation was $\sigma = 0.001$.

temperatures (dotted lines) and fluxes (dashed lines). These figures, generated for different values of input σ, serve to prove that neither the SVD nor Tikhonov's methods amplified the noise supplied in the input measurement data. The SVD was less oscillatory and more accurate than Tikhonov's scheme. We repeated these tests by introducing input noise into the outer boundary heat flux data to see if there would be any difference, but similar results were found.

In addition, global energy conservation requires that the integrated heat flux through the unspecified boundaries equals the sum of all fluxes entering and leaving the domain through the specified and overspecified boundaries plus any heat generated inside the domain.

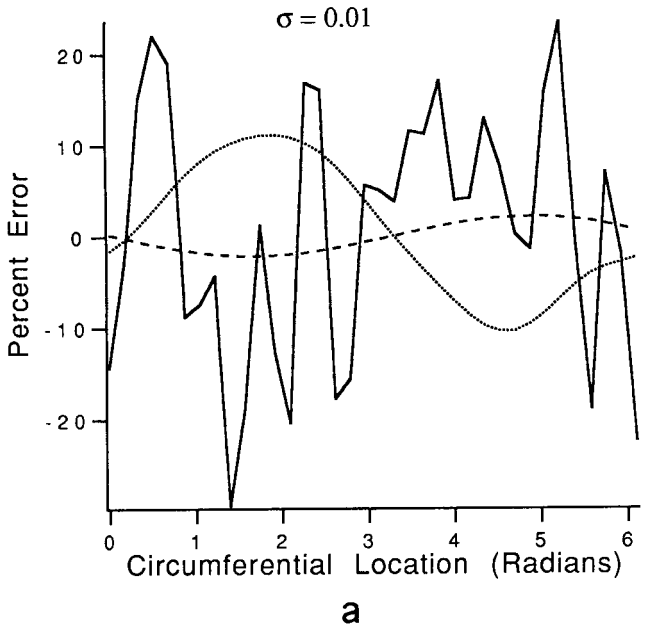

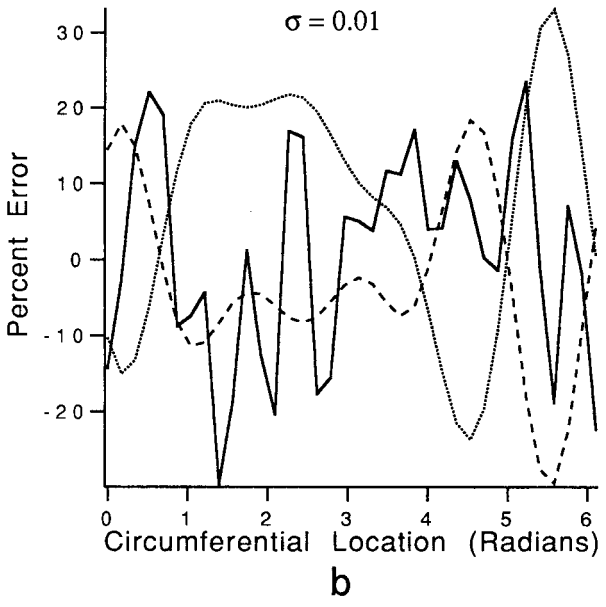

Fig. 6 Circumferential distribution of specified (input) percentage errors of nondimensional temperature on the outer circular boundary (full line) and computed (output) percentage errors in nondimensional temperature (dotted line) and heat flux (dashed line) on the inner circular boundary: (*a*) using the SVD algorithm, and (*b*) using Tikhonov's regularization. Input standard deviation was $\sigma = 0.01$.

$$Q_5 = \int_{\Gamma_5} (\nabla u_5 \cdot \hat{n}_5) d\Gamma$$

$$= -\left\{ \sum_{i=1}^{4} \left(\int_{\Gamma_i} (\nabla u_i \cdot \hat{n}_i) d\Gamma \right) + \int_{\Omega} b d\Omega \right\} \quad (23)$$

In our case, $b = 1$ and $Q_a = Q_5 = 2\pi\rho_a q_a = -\pi\{2\rho_b q_b + b(\rho_b^2 - \rho_a^2)\} = -1.35$. Again, a series of tests were performed for the same range of input standard deviations and the biases in the net heat fluxes on the unspecified boundary were computed with the SVD and Tikhonov methods.

The choice of Tikhonov's regularization parameter, λ, was found to affect Q_a strongly, although the amount of input standard deviation did not affect Q_a directly. Figure 7 readily shows that larger values of λ yielded a greater error in Q_a. Obviously, Tikhonov's regularization introduces artificial dissipation, which affects the physics of the problem by reducing the global amount of heat transfer. Since larger λ_{opt}'s are required for higher input variances, the results obtained with Tikhonov's regularization become increasingly biased as the input measurement data becomes more corrupted and noisy. A comparison between Figs. 3 and 7 indicates that this artificial dissipation of heat can become unacceptably large when using very noisy input data.

On the other hand, the SVD did not exhibit this behavior. Once the threshold parameter was small enough, the net heat flux, Q_a, became equal to the correct value and remained unchanged for all smaller values of τ.

We conclude from these observations that the SVD technique is more robust and reliable than Tikhonov's regularization since the latter can mislead the observer into thinking that a highly biased result is correct because it appears to be smooth. With the SVD, the user will immediately recognize if the chosen value of the threshold parameter, τ, is wrong since the computed temperatures and heat fluxes will be highly oscillatory. In addition, since the correct value of Q_5 is known in both well-posed and ill-posed problems, the value of τ_{opt} can be determined from this information after only 2–3 repetitive trials by starting with an initial guess $\tau < 0.1$. This is an easier procedure than with Tikhonov's method where λ_{opt} is found iteratively by simultaneously minimizing the variance and the bias. Even with this value of λ_{opt} Tikhonov's method will create results that have a nonzero bias, while the SVD approach offers a zero bias.

Results With an Arbitrary Heat Source Function. Our BEM algorithm was then tested against the complete analytic solution (Eq. (18)) for the same geometry, but with the nondimensional heat generation taken as a function of both the nondimensional radius, ρ, and azimuthal angle, θ. Specifically, we used the following expression:

$$b(\rho, \theta) = \sin\left[\frac{\rho - \rho_a}{\rho_b - \rho_a}\pi\right] \sin\theta \quad (24)$$

thus creating a variable heat source distribution on the upper

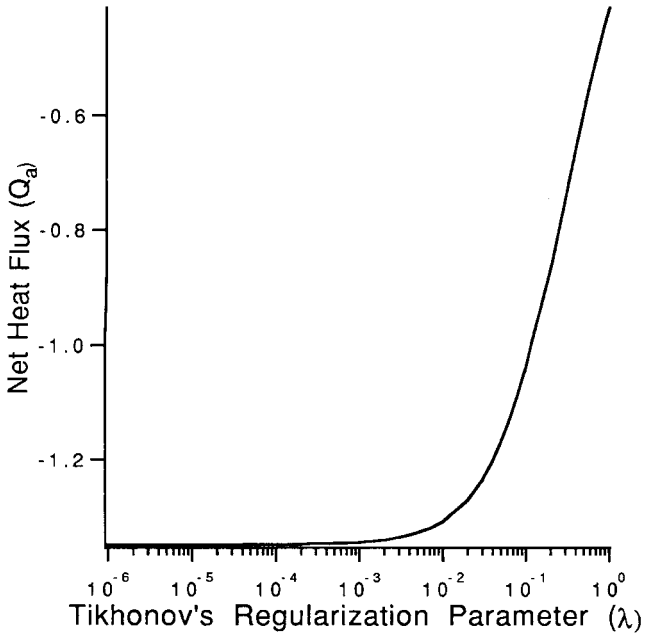

Fig. 7 Variation of the integrated net heat flux, Q_a, through the unspecified inner circular boundary as a function of Tikhonov's regularization parameters, λ. The nondimensional analytic result for the net heat flux is $Q_a = -1.35$.

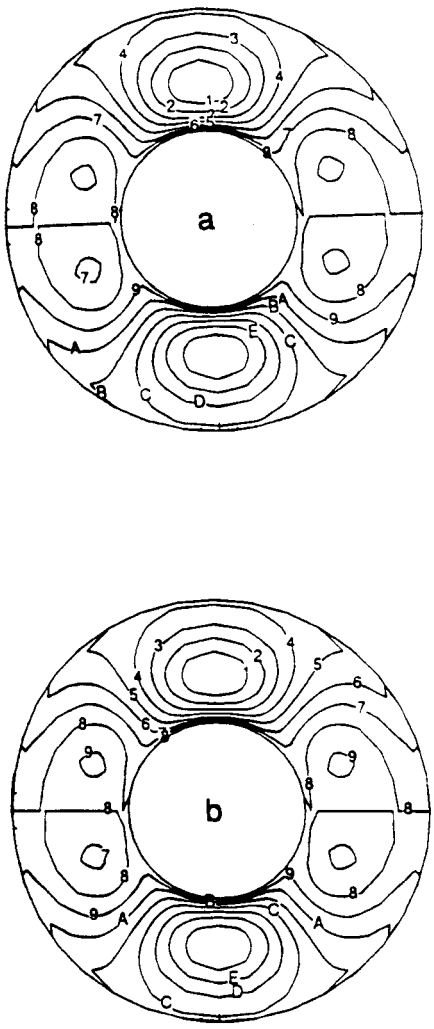

% error	
F	0.564803
E	0.484117
D	0.403431
C	0.322745
B	0.242058
A	0.161372
9	0.0806862
8	-7.450E-9
7	-0.0806862
6	-0.161372
5	-0.242058
4	-0.322745
3	-0.403431
2	-0.484117
1	-0.564803

% error	
F	0.564799
E	0.484113
D	0.403428
C	0.322742
B	0.242057
A	0.161371
9	0.0806856
8	-7.450E-9
7	-0.0806856
6	-0.161371
5	-0.242057
4	-0.322742
3	-0.403428
2	-0.484113
1	-0.564799

Fig. 8 Contours of constant error levels in computed nondimensional temperatures compared with the analytic results of the Poisson equation on an annular domain with $\rho_a = 0.5$, $\rho_b = 1.2$ and $b = \sin\{[(\rho - \rho_a)/(\rho_b - \rho_a)]\pi\} \sin\theta$: (a) error in numerical results obtained with the BEM for the direct problem ($u_a = 0.0$, $q_b = 0.0$); (b) error in numerical results obtained with the BEM for the inverse problem ($u_a = 0.0$, q_a = analytic, u_b = unknown, q_b = unknown)

half of the annular domain and an equal distribution of the heat sinks on the lower half of the annular domain. For the well-posed problem, the nondimensional temperature $u_a = 0$ was specified on the inner circular boundary while the outer circular boundary was kept adiabatic, $q_b = 0$. Both inner and outer boundaries were discretized with 36 linear isoparametric boundary elements and the annular domain was discretized with 36 $\times$ 10 quadrilateral cells. Accuracy of the numerical results obtained with our BEM analysis code for this well-posed test problem is very good (Fig. 8(a)). Next, the inner circular boundary heat fluxes were taken from the analytic solution (Eq. (18)) and supplied as overspecified boundary conditions together with nondimensional temperature on the inner circular boundary. No boundary conditions were specified on the outer circular boundary. This SIHCP was solved using our BEM code. The largest percentage errors found in the domain of the computed non-dimensional temperature field were less than 0.6 percent (Fig. 8(b)). Notice that the errors in both the direct (well-posed) and inverse (ill-posed) problems were nearly identical. The errors may seem to be somewhat larger near the boundaries because the singular fundamental solution is distributed over the boundary. A higher order integration scheme would alleviate this problem.

Results With Interior Temperature Measurements. The BEM approach to solving inverse (ill-posed) boundary condition problems is also capable of using internal temperature measurements at isolated interior points. To demonstrate this on the same annular geometry, only the temperature $u_a = 0$ was specified on the inner circular boundary. No boundary conditions were specified on the outer circular boundary. Instead, analytical values for temperatures at various locations within the domain were used as additional input data. Nondimensional temperatures ($u_{\text{int}} = 0.0496$), corresponding to the analytical values at $\rho = 1$ for Poisson's equation with the boundary conditions $u_a = 0$, $u_b = 0$, and $b = 1$, were specified at a finite number of circumferentially equidistantly spaced points in the annular domain. Each circular boundary was discretized with $M/2 = 36$ linear isoparametric boundary elements. A singularity threshold of $\tau = 0.06$ was used. Figure 9(a) illustrates the isotherms computed by the BEM algorithm when only four circumferentially and equidistantly spaced internal temperatures were utilized. The errors in the predicted temperature on the outer circular boundary are significant. This is understandable since the resulting BEM equation set contained 76 equations ($36 \times 2 + 4 = 76$) and 108 unknowns. The isotherms in Figs. 9(b) and 9(c) result from using 6 ($36 \times 2 + 6 = 78$ equations) and 9 ($36 \times 2 + 9 = 81$ equations) equidistantly spaced internal temperature input points, respectively. From these figures one notices that our algorithm produced very good results when at least 9 temperature measurements were used at equidistantly spaced locations within the annular domain while only temperature was given on one circular boundary.

Detection of the Heat Generation Inside an Annular Disk. In order to verify that the BEM is capable of finding the internal heat generation field given overspecified boundary data, we used the annular disk geometry described earlier with axisymmetric boundary conditions, $u_a = u_b = 0$ and $b = 1$. The resulting analytical values for the nondimensional heat fluxes on the outer and inner circular boundaries were $q_b = -0.3168$ and $q_a = -0.4296$, respectively.

These fluxes were then used as the overspecified boundary conditions on the outer and inner circular boundaries in order to predict the value of the heat generation field. The accuracy of the numerical solution was determined by how the internal region was discretized. The outer and inner circular boundaries were discretized with 36 linear isoparametric elements. When the annular domain (disk area) was discretized with 36 quadrilateral cells circumferentially, having only one cell between the outer and inner circular boundaries, the results were excellent. The heat generation field was predicted with an average error less than 0.01 percent. Similar results were found when the heat generation field was linearly varying, $b(\rho) = (\rho - \rho_a)/(\rho_b - \rho_a)$. But, when the domain was discretized with two or more radial rows of quadrilateral cells, the results produced errors that were, at worst, in error by about 30 percent. This is because the assembled BEM matrix had at least twice as many unknowns as it had equations. The results were significantly improved whenever internal temperature measurements were included in the analysis. For example, when the domain was discretized with two rows of quadrilateral cells, a single row of 9 known internal temperatures produced results that averaged an error of less than 0.1 percent.

Further results have shown that whenever the temperature field is entirely known everywhere in the domain, the resulting solution matrix, $[\mathbf{P}]$, is both square and well-conditioned. After inversion of this matrix, the unknown heat source vector $\{\mathbf{B}\}$ can be found with an accuracy comparable to the well-posed (forward) problem, where $\{\mathbf{B}\}$ is known and the temperature field is the objective of the computation.

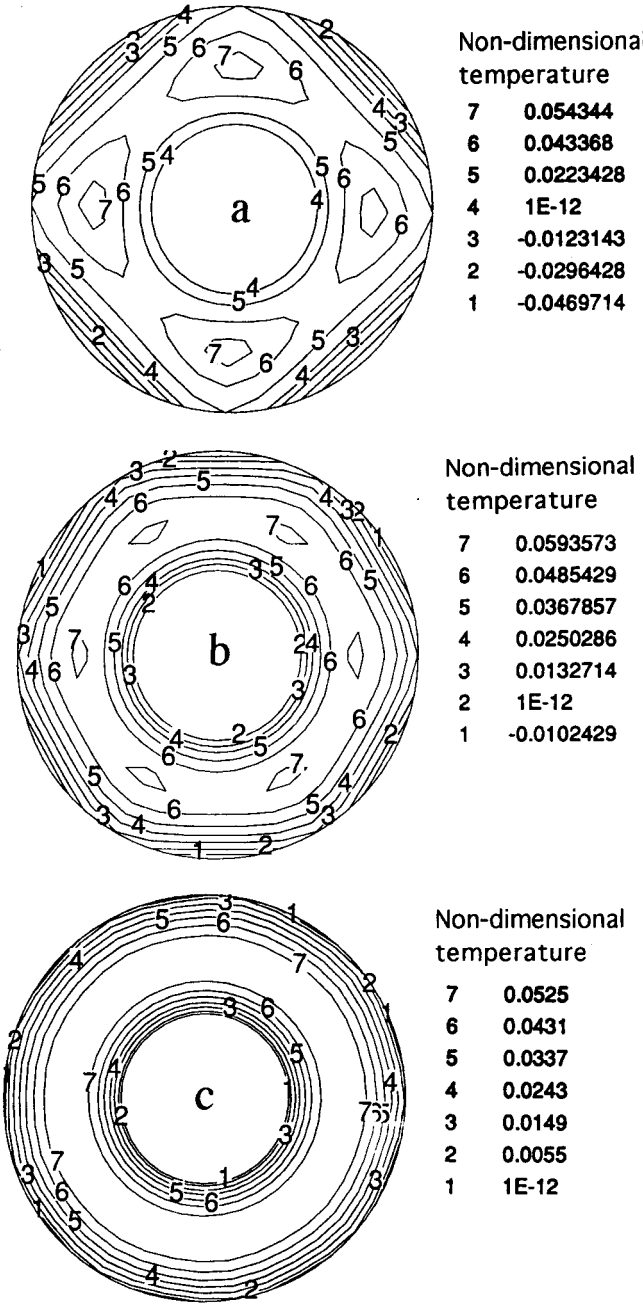

Fig. 9 Computed curves of constant nondimensional temperature in the annular region for the SIHCP with $b = 1.0$, $u_a = 0.0$, u_b = unknown, and local temperature measurements provided at: (a) four, (b) six, and (c) nine circumferentially equidistantly spaced points at $\rho = 1.0$

Conclusions

The BEM has been shown to provide stable and accurate solutions to several simple ill-posed problems of the Poisson equation where the boundary conditions or heat source functions were partially unknown and partially overspecified. Furthermore, this technique does not iterate to minimize a global function based upon the residual between the overspecified and computed boundary values. The magnification of errors in measurement data, the need for mollifiers to smooth the intermediate predictions, and the influence of regularizers on the physics of the problem have been eliminated. It was found that Singular Value Decomposition (SVD) technique is more reliable than Tikhonov's regularization for this class of ill-posed problems. This method can be readily extended to the solution of three-dimensional (Martin and Dulikravich, 1995) inverse (ill-posed) boundary condition problems governed by the Laplace and Poisson equations and to unsteady heat conduction problems involving the detection of unknown boundary conditions and initial conditions.

Acknowledgments

The authors are grateful for the remote access to NASA Ames Research Center (NAS) facility Cray C-90 computer granted by NASA Lewis Research Center. Postprocessing was performed on the equipment donated by Apple Computer. We also greatly appreciate Mr. Norman F. Foster's and Mr. Brian H. Dennis's help with the graphics and Mr. Sean R. Lynn's help with proofreading. The lead author is grateful for the NASA Graduate Traineeship received from the NASA-Pennsylvania State University Propulsion Engineering Research Center. This work was supported in part by NSF grant No. DMI-9522854 monitored by Dr. George Hazelrigg.

References

Backus, B., and Gilbert, F., 1970, "Uniqueness in the Inversion of Inaccurate Gross Earth Data," *Phil. Trans. Royal Soc. London,* Vol. 266, pp. 123–192.

Beck, J. V., Blackwell, B., and St. Clair, C. R., Jr., 1985, *Inverse Heat Conduction: Ill-Posed Problems,* Wiley-Interscience, New York.

Brebbia, C. A., 1978, *Boundary Elements in Engineering,* McGraw-Hill, New York.

Brebbia, C. A., and Dominquez, J., 1989, *Boundary Elements, An Introductory Course,* McGraw-Hill, New York.

Dulikravich, G. S., and Martin, T. J., 1994, "Inverse Problems and Design in Heat Conduction," *Proc. 2nd International Symposium on Inverse Problems in Engineering,* H. D. Bui, M. Tanaka, M. Bonnet, H. Maigre, E. Luzzato and M. Reynier, eds., Paris, France, Nov. 2–4, 1994; A. A. Balkema, Rotterdam, pp. 13–20.

Dulikravich, G. S., and Martin, T. J., 1995, "Inverse Shape and Boundary Condition Problems and Optimization in Heat Conduction," in: *Advances in Numerical Heat Transfer,* W. J. Minkowycz and E. M. Sparrow, eds., Taylor and Francis, Chap. 10.

Kagawa, Y., Sun, Y.-H., and Matsumoto, O., 1995, "Inverse Solution of Poisson Equation Using DRM Boundary Element Model—Identification of Space Charge Distribution," *Inverse Problems in Eng.,* Vol. 1, No. 3, pp. 247–266.

Lanczos, C., 1961, *Linear Differential Operators,* Van Nostrand, London.

Martin, T. J., and Dulikravich, G. S., 1993, "A Direct Approach to Finding Unknown Boundary Conditions in Steady Heat Conduction," *Proc. 5th Annual Thermal and Fluids Workshop,* Lewis Research Center, OH, Aug. 16–20, 1993, NASA CP-10122, pp. 137–149.

Martin, T. J., and Dulikravich, G. S., 1994, "Inverse Determination of Temperatures and Heat Fluxes on Inaccessible Surfaces," in: *Boundary Element Technology IX,* Computational Mechanics Publications, Southampton, C. A. Brebbia and A. Kassab, eds., pp. 69–76.

Martin, T. J., and Dulikravich, G. S., 1995, "Finding Temperatures and Heat Fluxes on Inaccessible Surfaces in 3-D Coated Rocket Nozzles," *Proc. 1994 JANNAF Propulsion and Subcommittee Joint Meeting,* Tampa, FL, Dec. 4–8.

Martin, T. J., Halderman, J., and Dulikravich, G. S., 1994, "An Inverse Method for Finding Unknown Surface Tractions and Deformations in Elastostatics," *Symposium on Inverse Problems in Mechanics,* S. Saigal and L. G. Olson, eds., ASME AMD-Vol. 186, pp. 57–66; also in *Computers and Structures,* Vol. 56, No. 5, Sept. 1995, pp. 825–836.

Murio, D. A., 1993, *The Mollification Method and the Numerical Solution of Ill-Posed Problems,* Wiley, New York.

Press, W. H., Teukolsky, S. A., Vetterling, W. T., and Flannery, B. P., 1992, *Numerical Recipes in FORTRAN,* 2nd ed., Cambridge University Press.

Sykulski, J. K., ed., 1995, *Computational Magnetics,* Chap. 5 (authored by K. Pawluk), Chapman & Hall, London.

Throne, R. D., and Olson, L. G., 1994, "A Generalized Eigensystem Approach to the Inverse Problem of Electrocardiography," *IEEE Transactions on Biomedical Engineering,* Vol. 41, No. 6, pp. 1–9.

Tikhonov, A. N., 1977, *Solutions of Ill-Posed Problems,* Halsted Press, Washington–Winston–New York.